Inorganic Chemistry

Article

pubs.acs.org/IC

# Structural Factors That Enhance Lithium Mobility in Fast-Ion $Li_{1+x}Ti_{2-x}Al_x(PO_4)_3$ ($0 \leq x \leq 0.4$) Conductors Investigated by Neutron Diffraction in the Temperature Range 100−500 K

K. Arbi,[†] M. Hoelzel,[‡] A. Kuhn,[§] F. García-Alvarado,[§] and J. Sanz*,[†]

[†]Instituto de Ciencia de Materiales Madrid (CSIC), 28049 Cantoblanco, Madrid, Spain

[‡]Forschungsneutronenquelle Heinz-Maier-Leibnitz (FRM II), Technische Universität München, Lichtenbergstrasse 1, D-85747 Garching, Germany

[§]Facultad de Farmacia, Department of Chemistry, Urbanizacion Montepríncipe, Universidad CEU San Pablo, 28668 Boadilla del Monte, Madrid, Spain

Supporting Information

**ABSTRACT:** Structural features responsible for lithium conductivity in $Li_{1+x}Ti_{2-x}Al_x(PO_4)_3$ ($x$ = 0, 0.2, and 0.4) samples have been investigated by Rietveld analysis of high-resolution neutron diffraction (ND) patterns. From structural analysis, variation of the Li site occupancies and atomic thermal factors have been deduced as a function of aluminum doping in the temperature range 100−500 K. Fourier map differences deduced from ND patterns revealed that Li ions occupy M1 sites and, to a lower extent, M3 sites, disposed around ternary axes. The occupation of M1 sites by Li ions is responsible for the preferential expansion of the rhombohedral $R\bar{3}c$ unit cell along the $c$ axis with temperature. The occupation of less symmetric M3 sites decreases electrostatic repulsions among Li cations, favoring ion conductivity in $Li_{1+x}Ti_{2-x}Al_x(PO_4)_3$ compounds. The variations detected on long-range lithium motions have been related to variations of the oxygen thermal factors with temperature. The information deduced by ND explains two lithium motion regimes deduced previously by $^7$Li NMR and impedance spectroscopy.

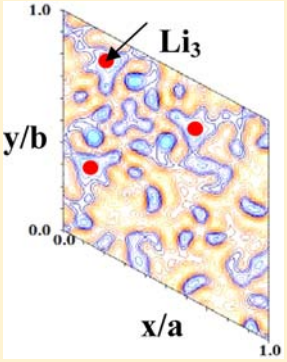


## INTRODUCTION

Li-ion batteries (LIBs) based on solid electrolytes are one of the most promising stationary power sources for sustainable energy storage. The performance of LIBs depends critically on the materials used; thus, the preparation of new cheaper and safer materials is crucial for developing new-generation LIBs required for large-scale applications in electric and hybrid electric vehicles.[1−4] However, before LIBs can be used in high-power applications, some characteristics regarding the battery cycle life, rate capability, production cost, and safety must be improved.

In all-solid-state LIBs, the solid electrolyte is one of the key components that control the properties of the batteries. Solid electrolytes must meet certain requirements including high conductivity, large cationic transport number, wide potential window, and low electronic conductivity. Lithium phosphates are between active materials able to answer safety concerns surrounding oxide chemistry.[5] Among phosphates, good electrochemical performances have been reported for Nasicon-type materials, proposed as electrodes and/or electrolytes for secondary LIBs.[6,7]

The Nasicon framework of $LM_2(PO_4)_3$ (L = Li and Na and M = Ge, Ti, Sn, Hf, and Zr) materials is built up by $M_2(PO_4)_3$ units, in which two $MO_6$ octahedra share O atoms with three $PO_4$ tetrahedra.[8,9] Tetrahedra and octahedra of contiguous $M_2(PO_4)_3$ units are bound to form the three-dimensional network of Nasicon phases (Figure 1). The usual symmetry of

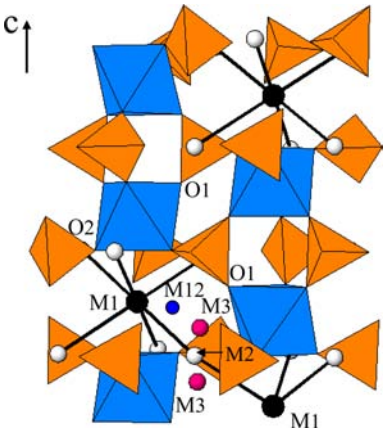


**Figure 1.** Structure of Nasicon compounds displaying M1, M12, M2, and M3 Li sites along conduction channels (connected lines).

$LiM_2(PO_4)_3$ compounds is rhombohedral $R\bar{3}c$, although in some cases, a triclinic distortion (space group $C\bar{1}$) was found.[10−14] In rhombohedral samples, $Li^+$ ions are usually surrounded by six O atoms in M1 sites,[10,11] but in triclinic phases, $Li^+$ ions are 4-fold-coordinated at M12 sites between M1 and M2 positions (Figure 1).[12−14]

**Received:** March 7, 2013
**Published:** July 30, 2013

   dx.doi.org/10.1021/ic400577v | Inorg. Chem. 2013, 52, 9290−9296

The ionic conductivity of the $LiM_2(PO_4)_3$ series is considerably enhanced, reaching values near $10^{-3}$ S cm$^{-1}$ at room temperature, when the tetravalent ions (M) are partially substituted by trivalent cations (Al, Ga, In, Fe, etc.).[15−19] In Li-intercalated $Li_3Ti^{3+}{}_2(PO_4)_3$ samples, diffraction patterns were indexed with the rhombohedral space group $R\bar{3}$ and Li ions were disposed near M2 sites, in two different M3 and M3′ positions.[20−22] In these materials, the creation of vacancy at the conduction pathway crossing (M1 sites) was suggested to improve long-range lithium mobility (Figure 1).[23]

In the present work, structural features of $Li_{1+x}Ti_{2-x}Al_x(PO_4)_3$ compounds have been deduced from the Rietveld analysis of neutron diffraction patterns recorded in the 100−500 K interval. Fourier map differences have been used to localize Li ions in the Nasicon framework. In this work, special attention has also been paid to analyze structural reasons that favor lithium mobility. The correlation between structural information, deduced by neutron diffraction, and lithium mobility, deduced by impedance and NMR spectroscopy,[23] provides new insight about the origin of lithium conductivity in Nasicon materials.

## EXPERIMENTAL SECTION

The $Li_{1+x}Ti_{2-x}Al_x(PO_4)$ samples were prepared by heating stoichiometric mixtures of $Li_2CO_3$, $(NH_4)_2H(PO_4)_3$, $Al_2O_3$, and $TiO_2$ at increasing temperatures in the 573−1373 K interval, following the procedure described elsewhere.[24,25]

X-ray diffraction patterns of powder samples were analyzed with Cu K$\alpha$ radiation ($\lambda$ = 1.54056 Å) in a Phillips PW 1050/25 apparatus to identify crystalline phases. Unit cell parameters of the $Li_{1+x}Ti_{2-x}Al_x(PO_4)_3$ samples, with nominal $x$ = 0, 0.2, and 0.4 values, were determined with the *Fullprof* package.[26] In order to increase the sensitivity to O and Li positions, neutron diffraction (ND) patterns were collected in the high-resolution powder SPODI diffractometer of the FRM-II reactor (Garching, Munich, Germany). In this analysis, a wavelength of 1.548 Å was selected from the germanium monochromator. Cylindrical vanadium cans of 8 mm diameter were filled with 2 g of powder sample and mounted in a high-temperature vacuum furnace equipped with niobium heating elements. ND patterns were collected for 4 h over the $2\theta$ = 5−160° range with a step size of 0.05°.

In structural analyses carried out with the Rietveld method, a pseudo-Voigt function was chosen to reproduce the line shape of the diffraction peaks.[27] In $Li_{1+x}Ti_{2-x}Al_x(PO_4)_3$ structural refinements, the $R\bar{3}c$ model, given in Table 1, was used. Neutron coherent lengths used for Li, Ti, Al, P, and O atoms were −1.90, −3.30, +3.45, +5.13, and +5.80 fm.[28] The negative length factors of the Ti and Li atoms increase considerably the contrast of Ti and light O and Li elements, making favorable Fourier map investigations addressed to localize Li atoms. Rietveld analysis performed on ND patterns recorded between 100 and 500 K afforded relevant information about the evolution of the atom thermal factors and Li site occupancies with temperature.

**Table 1. $R\bar{3}c$ Model Used in the Structural Refinement of ND Patterns of $Li_{1+x}Ti_{2-x}Al_x(PO_4)_3$**

| atom | Wyckoff position | $x/a$ | $y/b$ | $z/c$ | occupancy |
|---|---|---|---|---|---|
| Li1 | 6b | 0 | 0 | 0 | 1 |
| Li3 | 36f | 0.070 | 0.34 | 0.07 | 0.2 |
| Ti, Al | 12c | 0 | 0 | 0.142 | 1 |
| P | 18e | 0.290 | 0 | $^1/_4$ | 1 |
| O1 | 36f | 0.185 | 0.996 | 0.190 | 1 |
| O2 | 36f | 0.188 | 0.164 | 0.081 | 1 |

## RESULTS

ND patterns of three analyzed $Li_{1+x}Ti_{2-x}Al_x(PO_4)_3$ samples are depicted in Figure 2. In all cases, ND patterns display the Nasicon $R\bar{3}c$ symmetry; however, in the Al-rich $x$ = 0.4 sample, additional peaks at 21.9, 31.3, 38.4, 46.8, 56.8, 61.7, and 88.9° ($2\theta$) indicate the presence of aluminum phosphates as minor secondary phases (less than 4% by weight).

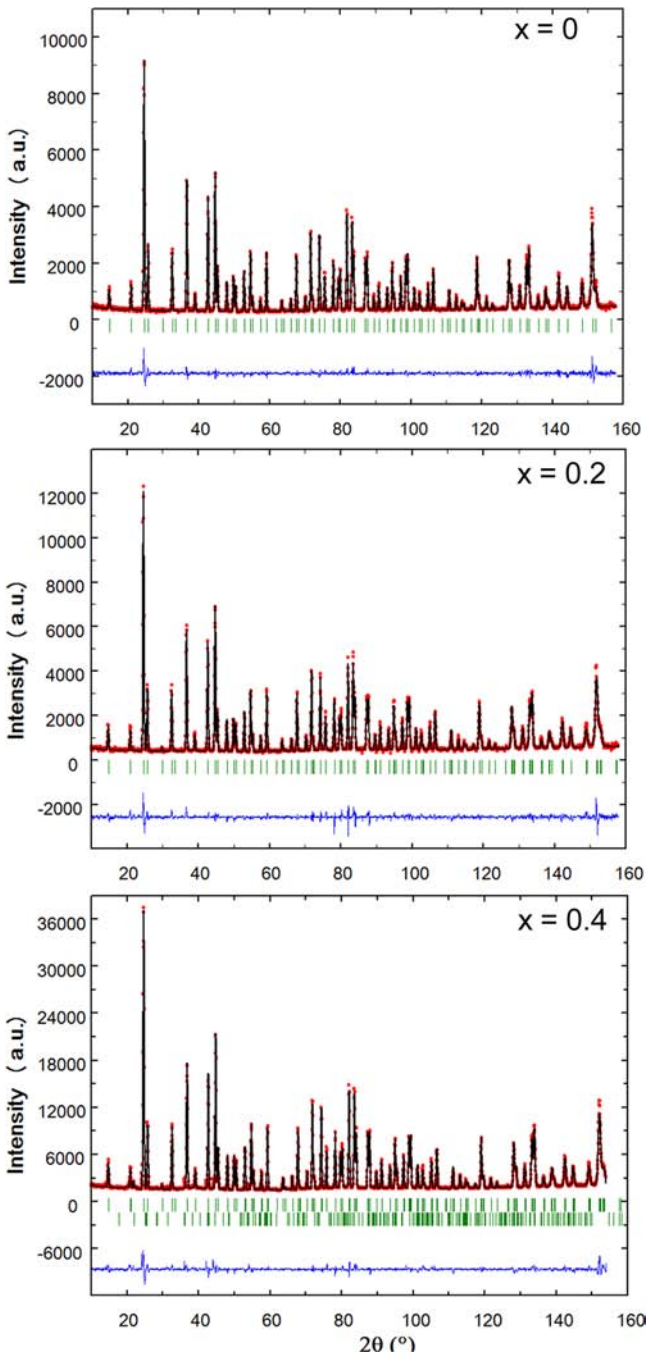


**Figure 2.** ND pattern of the $Li_{1+x}Ti_{2-x}Al_x(PO_4)_3$ ($x$ = 0, 0.2, and 0.4) samples, recorded at 295 K, where observed, calculated, and difference profiles are depicted. Bragg positions deduced from the $R\bar{3}c$ model are marked with vertical lines. In the case of the $Li_{1.4}Ti_{1.6}Al_{0.4}(PO_4)_3$ sample, peaks of secondary $AlPO_4$ phases were detected.

In structural analyses carried out with the *Fullprof* program, the overall parameters histogram scale factors, background


dx.doi.org/10.1021/ic400577v | Inorg. Chem. 2013, 52, 9290−9296

coefficients, unit cell parameters, zero-shift errors, and pseudo-Voigt coefficients[29] corrected for asymmetry[30] were first refined. The temperature dependence of the unit cell parameters $a$ and $c$ is given in Figure 3. It is observed that

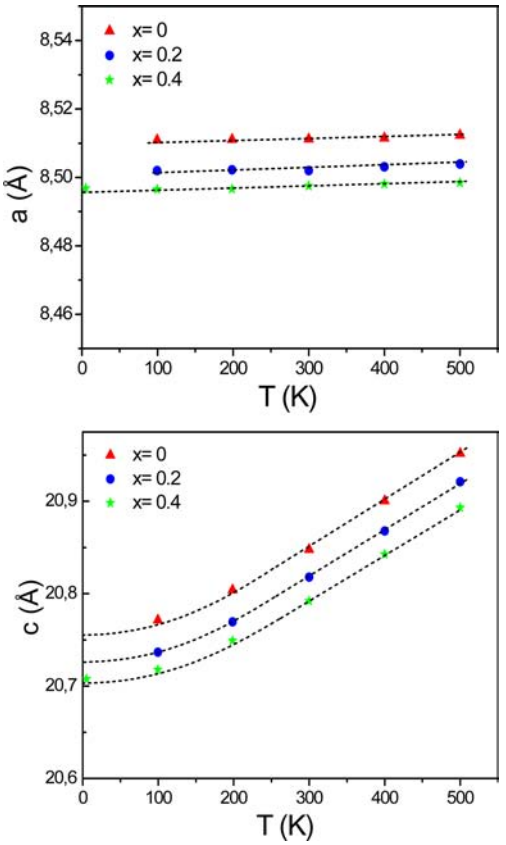


**Figure 3.** Temperature dependence of the unit cell parameters $a$ and $c$ of the $Li_{1+x}Ti_{2-x}Al_x(PO_4)_3$ ($x$ = 0, 0.2, and 0.4) samples.

both parameters decrease with the incorporation of Al into the Nasicon framework. The heating of samples produced anisotropic expansion of the unit cell: the increment of the $a$ axis is small, but that of the $c$ axis is considerably larger. The expansion coefficients deduced for the $a$ and $c$ axes are ~3.33 × $10^{-6}$ and 4.13 × $10^{-4}$ Å $K^{-1}$, respectively.

In structural refinements carried out with the Rietveld method, positional parameters were first deduced; then the site occupations and isotropic thermal parameters of the atoms were determined. Structural information deduced for the $Li_{1+x}Ti_{2-x}Al_x(PO_4)_3$ samples is given as Supporting Information in Tables SM1−3.

The total amount of aluminum incorporated in the Nasicon framework was lower than the nominal one. In the case of $Li_{1.2}Ti_{1.8}Al_{0.2}(PO_4)_3$, the amount of aluminum was 0.17, but in the case of $Li_{1.4}Ti_{1.6}Al_{0.4}(PO_4)_3$, this amount was 0.27, indicating, in agreement with previous results,[24] that the amount of aluminum segregated as aluminum phosphates increases above $x$ = 0.2.

In the samples analyzed here, it was found that the Li site occupation of M1 sites decreases with the amount of incorporated aluminum. In order to investigate other possible sites for lithium, the Fourier map differences between observed peaks and intensities deduced from structural models without Li and with Li occupying M1 sites were calculated (Figure 4). In both cases, negative peaks for Li at M1 (0, 0, 0) and M3 (0.06, 0.34, 0.08) positions were detected. The incorporation of lithium at these two sites considerably improved the agreement factors and considerably decreased its contribution to the Fourier map differences at sections $z$ = 0 (Figure 4a,b) and $z$ = 0.0625 (Figure 4c,d). The existence of correlations between site occupancies and thermal factors of lithium overestimated the overall lithium content of the samples;[31] to limit this effect, thermal Li1 and Li3 factors were assumed to be equal and the lithium content per formula was constraint to 1 + [Al] values.

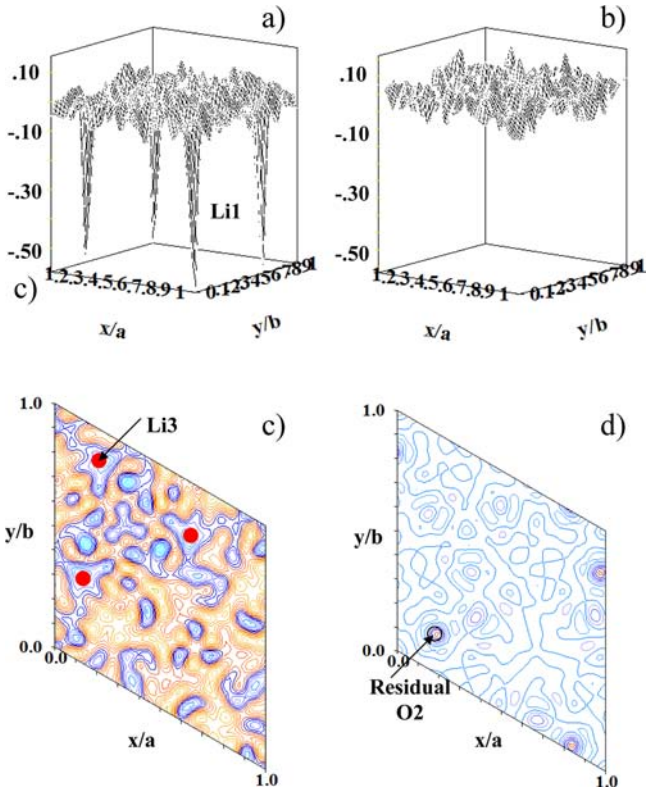


**Figure 4.** Fourier map differences calculated at $z/c$ = 0 from ND patterns recorded at 5 K. In this calculation, structural $R\bar{3}c$ models without Li (a) and with Li (b) occupying M1 sites were considered. New negative peaks were detected for Li at M1 (0, 0, 0) and M3 (0.06, 0.34, 0.07) positions (a and c). The incorporation of lithium at two sites considerably decreased the contribution of lithium to the Fourier map differences at $z/c$ = 0.062 (d).

The compositional dependence of Li1 and Li3 site occupation is analyzed in Figure 5. It can be observed that the increment of lithium slightly reduces the amount of Li at M1 sites but considerably increases that at M3 sites. This result suggests that the increment of lithium increases electrostatic repulsions between Li cations, destabilizing the occupancy of M1 sites. The increment of temperature showed an appreciable decrement on the M3 site occupancy but a moderate effect on the M1 site occupancy, indicating that Li is better stabilized at M1 sites than at M3 sites.

A summary of the mean Li−O, Ti,Al−O, and P−O distances, measured at increasing temperatures, is depicted in Table 2. In general, the average P−O distances do not change, but the Ti,Al−O distances slightly decrease with the aluminum content. Small increments detected in the Li−O distances during heating of samples have been ascribed to enhancement of the lithium mobility.

Analysis of the atomic thermal factors is illustrated in Figures 6 and 7. In all cases, the thermal factors increase with the


dx.doi.org/10.1021/ic400577v | Inorg. Chem. 2013, 52, 9290−9296

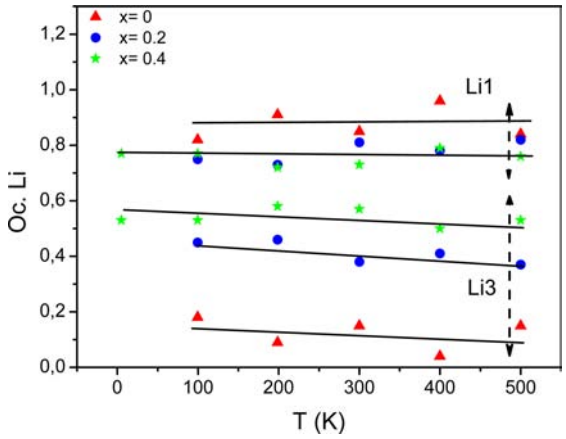


**Figure 5.** Temperature dependence of Li1 and Li3 site occupation in $Li_{1+x}Ti_{2-x}Al_x(PO_4)_3$ ($x$ = 0, 0.2, and 0.4) samples.

amount of aluminum and temperature. In the case of P tetrahedra, the temperature dependence of the $B_P$ factors is linear and moderate; however, that displayed by octahedral cations, $B_{Ti,Al}$, is not linear and considerably increases above 200 K (Figure 6a,b). In the case of O atoms, $B_{O1}$ and $B_{O2}$ display a similar dependence; however, the temperature dependence of $B_{O1}$ is appreciably higher than that of $B_{O2}$ (Figure 7a). The temperature dependence of $B_{Li}$ is much bigger than that detected for other cations, indicating an important contribution of the lithium mobility to this parameter (Figure 7b).

## DISCUSSION

Analysis of the unit cell parameters of the $Li_{1+x}Ti_{2-x}Al_x(PO_4)_3$ compounds indicates that the substitution of $Ti^{4+}$ by $Al^{3+}$ and $Li^+$ decreases the $c$ axis but only slightly affects the $a$ axis (Figure 3). The increment of octahedral aluminum slightly decreases the Ti,Al−O distances from 1.93 to 1.92 Å but does not appreciably affect the P−O distances, 1.53 Å (Table 2). The decrease of the mean cation size produces the progressive contraction of octahedra along the $c$ axis.

The increment of temperature from 100 to 500 K favors the preferential expansion of the $c$ axis with respect to the $a$ axis, increasing the volume of the unit cell. In the case of P and Ti,Al polyhedra, the P−O and Ti,Al−O distances do not appreciably change, but in the case of Li atoms, the Li−O distances considerably increase with temperature: Li1−O increases from 2.25 to 2.29 Å and Li2−O from 2.17 to 2.30 Å. Structural

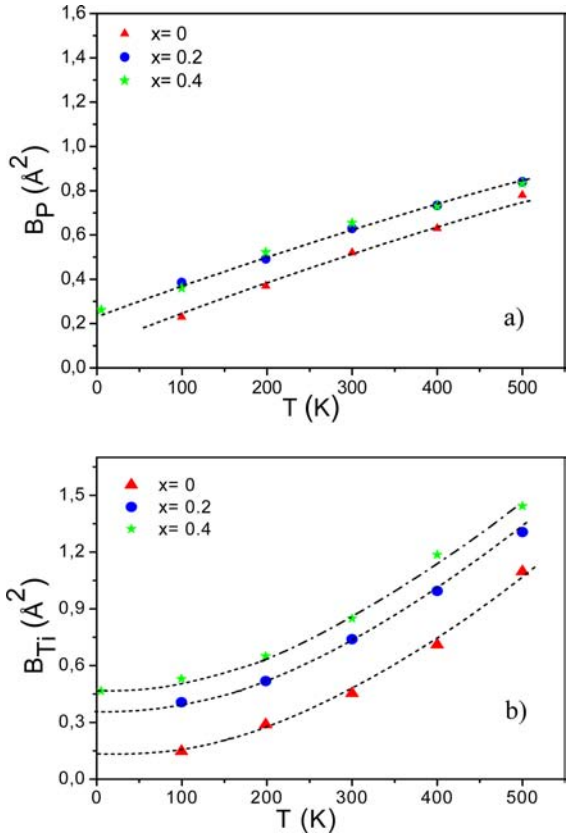


**Figure 6.** Temperature dependence of the $B_P$ (a) and $B_{Ti}$ (b) parameters in the $Li_{1+x}Ti_{2-x}Al_x$ $(PO_4)_3$ ($x$ = 0, 0.2, and 0.4) samples.

analyses indicate that the contribution of Li1 octahedra to the expansion of the $c$ axis is preponderant.

Rietveld analysis of the ND patterns indicates that the aluminum contents are always lower than nominal values. In samples with nominal $x$ values 0.2 and 0.4, aluminum contents deduced from structural refinements were 0.17 and 0.27. Observed differences increased with the amount of aluminum, suggesting that the limited miscibility of titanium and aluminum detected is mainly due to the formation of segregated $AlPO_4$ phases. Taking into account the charge balance, the amount of lithium incorporated into these compounds is limited to 1 + [Al] per structural formula.

**Table 2. Temperature Dependence of the Mean Li−O, Ti,Al−O, and P−O Distances (Å) in the $Li_{1+x}Ti_{2-x}Al_x(PO_4)_3$ ($x$ = 0, 0.2, and 0.4) Samples**

| | 5 K | 100 K | 200 K | 300 K | 400 K | 500 K |
|---|---|---|---|---|---|---|
| Li1−O (Al = 0.0) | | 2.24(2) | 2.26(2) | 2.27(2) | 2.27(2) | 2.29(2) |
| Li3−O | | 2.17(2) | 2.18(2) | 2.15(2) | 2.23(2) | 2.25(2) |
| Ti,Al−O | | 1.93(1) | 1.93(1) | 1.94(1) | 1.93(1) | 1.93(1) |
| P−O | | 1.53(1) | 1.53(1) | 1.53(1) | 1.53(1) | 1.53(1) |
| Li1−O (Al = 0.2) | | 2.25(2) | 2.26(2) | 2.27(2) | 2.28(2) | 2.29(2) |
| Li3−O | | 2.16(2) | 2.19(2) | 2.21(2) | 2.20(2) | 2.22(2) |
| Ti,Al−O | | 1.92(1) | 1.92(1) | 1.93(1) | 1.93(1) | 1.92(1) |
| P−O | | 1.53(1) | 1.53(1) | 1.53(1) | 1.52(1) | 1.53(1) |
| Li1−O (Al = 0.4) | 2.25(2) | 2.25(2) | 2.26(2) | 2.27(2) | 2.28(2) | 2.29(2) |
| Li3−O | 2.23(2) | 2.24(2) | 2.22(2) | 2.23(2) | 2.25(2) | 2.30(2) |
| Ti,Al−O | 1.92(1) | 1.92(1) | 1.92(1) | 1.92(1) | 1.92(1) | 1.92(1) |
| P−O | 1.53(1) | 1.53(1) | 1.53(1) | 1.52(1) | 1.53(1) | 1.53(1) |


dx.doi.org/10.1021/ic400577v | Inorg. Chem. 2013, 52, 9290−9296

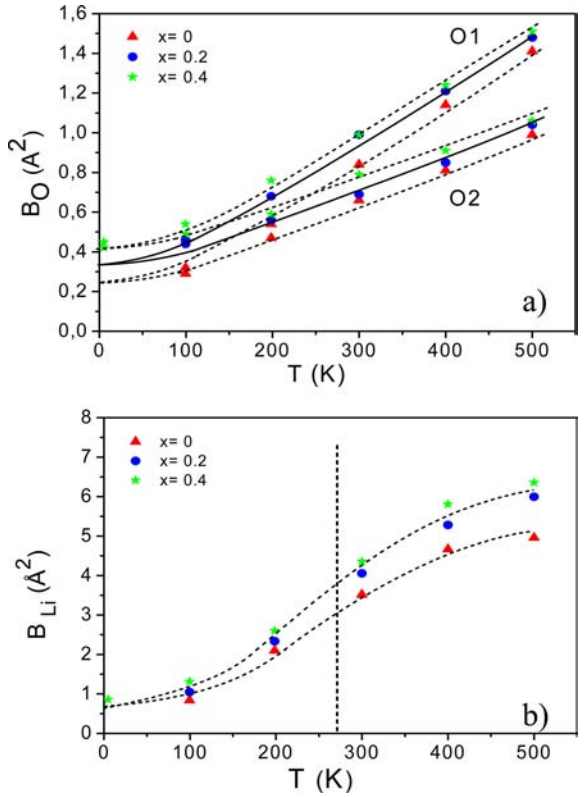


**Figure 7.** Temperature dependence of the $B_O$ (a) and $B_{Li}$ (b) parameters in the $Li_{1+x}Ti_{2-x}Al_x(PO_4)_3$ ($x$ = 0, 0.2, and 0.4) samples. In rhombohedral phases, O2 atoms are bound to Li1 ions.

On the other hand, the occupation of M1 sites by Li atoms is lower than that reported in $LiTi_2(PO_4)_3$, where the preferential occupation of 6-fold-coordinated M1 sites was detected.[21] In order to investigate alternative sites for Li, Fourier map differences between observed intensities and those calculated with the $R\bar{3}c$ model were studied. In this analysis, it was shown that, besides M1 sites, Li ions occupy M3 sites (0.07, 0.34, 0.07), previously proposed by Catti et al. in $Li_{1.5}Fe_{0.5}Ti_{1.5}(PO_4)_3$[31] and Aatiq et al. in $Li_3Ti_2(PO_4)_3$[21] (Figure 4). The partial occupation of M1 and M3 sites considerably improved structural refinements. As deduced in previous works, the lithium coordination at M3 sites is 4 + 1; however, the mean Li−O distances given in Table 2 have been calculated assuming a 4-fold distorted coordination for lithium. In three analyzed samples, the Li1−O distances deduced at 300 K were near 2.27 Å, but the Li3−O distances increased from 2.15 to 2.23 Å with the aluminum content.

In structural analyses performed in this work, it was observed that, for increasing lithium contents, the Li1 occupancy decreased and Li3 increased (Tables SM1−3 in the Supporting Information and Figure 5). The increment of the lithium content at M3 sites increases electrostatic Li1−Li3 repulsions; then, to minimize this interaction, Li was preferentially allocated at M3 sites. This arrangement increases the average distance Li3−Li3 (∼6 Å) with respect to that of Li1−Li3 ions (∼3 Å) in conduction channels.

Analysis of the thermal factors indicates that structural disorder and local motions contribute to $B$ parameters. In analyzed compounds, structural titanium and aluminum disorder explains important thermal $B_{Ti,Al}$ factors extrapolated to 0 K. Analysis of the temperature dependence of thermal factors affords valuable information about the local atom motion. This analysis shows that the local mobility of P ion is lower than that of Ti and Al cations and that of octahedral cations is considerably lower than that of Li ions (Figures 6 and 7). In analyzed samples, the lithium mobility increases slowly at low temperatures but faster above 200 K. Similar variations have been deduced for O atoms, suggesting that oxygen thermal motions affect lithium coordination. In three analyzed samples, the increment of $B_{O2}$ factors is appreciably lower than that of $B_{O1}$, suggesting that coordination of Li1 to O2 is more stable than that of Li3 to O1 and O2 atoms. On the basis of these observations, the local mobility of Li3 should be higher than that of Li1 ions; however, in refinements, the lithium thermal factors of Li1 and Li3 sites were assumed to be equivalent.

Structural information deduced from ND patterns was compared with that deduced by NMR and impedance spectroscopy in $Li_{1+x}Ti_{2-x}Al_x(PO_4)_3$ compounds.[23,24] Magic-angle-spinning $^7$Li NMR ($I = {}^3/_2$) spectra recorded below 250 K display three expected transitions modulated by the sample spinning (inset of Figure 8a). The increment of $C_Q$ values

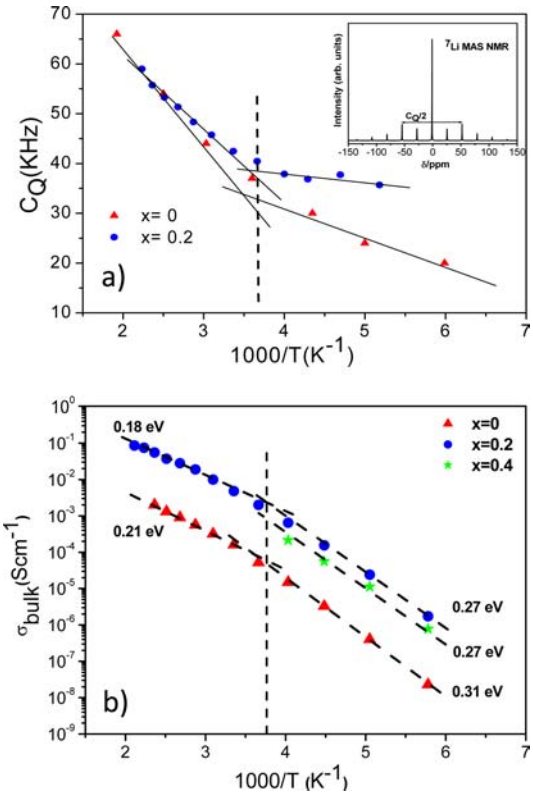


**Figure 8.** (a) Temperature dependence of quadrupolar $C_Q$ constants deduced from $^7$Li NMR spectra. (b) Inverse temperature dependence of bulk dc conductivity of the $Li_{1+x}Ti_{2-x}Al_x(PO_4)_3$ ($x$ = 0, 0.2, and 0.4) samples.

detected above 250 K, associated with quadrupolar interaction of lithium moments with electric field gradients at occupied sites, suggests the existence of Li exchange between M1 and M3 sites (Figure 8a). According to this mechanism, $C_Q$ values increase with the relative amount of Li located at distorted M3 sites, detecting a new regime at 250 K in $Li_{1.2}Ti_{1.8}Al_{0.2}(PO_4)_3$ and at 280 K in $LiTi_2(PO_4)_3$.[24]


dx.doi.org/10.1021/ic400577v | Inorg. Chem. 2013, 52, 9290−9296

Two regimes were also deduced from the temperature dependence of bulk conductivity (Figure 8b).[23] At low temperature, an activation energy of 0.27 eV was deduced in aluminum-doped samples, which was appreciably lower than that obtained in $LiTi_2(PO_4)_3$, 0.31 eV. At increasing temperatures, decrements in the activation energy from 0.31 to 0.21 eV and from 0.27 to 0.18 were observed in titanium- and aluminum-doped samples. This decrement has been ascribed to the increment of the conductivity detected above 250 K, which was previously ascribed to the creation of M1 vacant sites.[23]

These two regimes should be related to variation of the oxygen thermal factors $B_O$ with temperature. On the basis of structural refinements, the increment detected on the lithium mobility is triggered by oxygen local motions. According to observed variations, the oxygen thermal factors remain moderate below 250 K but increase considerably above this temperature. This variation agrees with that observed in $B_{Li}$, suggesting that local oxygen motions destabilize lithium coordination. A comparison of the $B_{O1}$ and $B_{O2}$ factors with temperature indicates that the local mobility of Li3 is higher than that of the Li1 species.

In general, direct-current (dc) conductivity depends on the structural site occupancy involved in hopping processes. The local mobility of lithium increases with temperature, but long-range motion requires the existence of vacant M1 sites at the intersection of conduction pathways. In general, the percolation of vacancies in three-dimensional networks is attained when the amount of vacancies per structural site is ~0.31.[32] In order to investigate this point, the occupation of M1 and M3 sites was analyzed as a function of the composition and temperature. In this analysis, it is observed that the amount of vacancies increases with the amount of lithium, approaching the percolation threshold in aluminum-richer samples. The detection of an important conductivity in samples with a lower amount of vacancies must be ascribed to the creation/elimination of vacancies during lithium motions.

In agreement with NMR and conductivity results,[23,24] the variation of $B_{Li}$ with temperature is higher in aluminum-doped $Li_{1+x}Ti_{2-x}Al_x(PO_4)_3$ than in the end member $LiTi_2(PO_4)_3$. In all cases, lithium thermal factors increase above 250 K, achieving a maximum at 500 K. The increment of lithium thermal factors was associated with the progressive delocalization of Li ions in ...M1−M3−M1... conduction paths. The long-range motion of lithium detected at high temperatures favors the detection of a new lithium signal at 0 ppm, displaying a much lower quadrupolar coupling.

Finally, when the conductivities of the samples are compared, it is observed that the conductivity increases from $x = 0$ to 0.2 but does not change significantly from 0.2 to 0.4. Analysis of the samples revealed similar structural features, suggesting, in agreement with previous works, that the presence of $AlPO_4$ could decrease the particles connectivity, affecting the long-range mobility of lithium.[24]

## CONCLUSIONS

Structural analysis of the $Li_{1+x}Ti_{2-x}Al_x(PO_4)_3$ ($x = 0$, 0.2, and 0.4) samples, prepared by the ceramic route, was performed in the temperature range 100−500 K. In all cases, samples display rhombohedral $R\bar{3}c$ symmetry. Structural refinements carried out in three samples at increasing temperatures showed that variations in the octahedral Li1−O and Ti,Al−O distances are responsible for the preferential expansion/contraction of the unit cell along the $c$ axis.

Fourier map differences deduced from high-resolution ND patterns revealed that Li ions occupy preferentially M1 sites in $LiTi_2(PO_4)_3$ samples but M1 and M3 sites in aluminum-doped samples. The increment of the lithium content favors the occupation of M3 sites, decreasing electrostatic repulsions between Li1 and Li3 ions. The creation of vacancies at M1 sites favors the onset of the fast conduction regime.

Rietveld analysis of the ND patterns revealed that the lithium mobility increases with the lithium content and temperature. Below 250 K, local exchange processes dominate lithium conductivity; but above 250 K, extended lithium motions were produced. The information deduced on oxygen thermal factors explains two lithium motion regimes detected by $^7$Li NMR and impedance spectroscopy. In general, the increment of $B_O$ factors destabilize the lithium coordination at M1 sites, improving the long-range mobility of lithium.

## ASSOCIATED CONTENT

### Supporting Information

Tables of structural parameters deduced from powder ND patterns. This material is available free of charge via the Internet at http://pubs.acs.org.

## AUTHOR INFORMATION

### Corresponding Author

*E-mail: jsanz@icmm.csic.es.

### Notes

The authors declare no competing financial interest.

## ACKNOWLEDGMENTS

Authors thank MINECO (Project MAT2010-19837-C06) and the regional government (Project S-2009/PPQ 1626) for financial support. K.A. thanks the Spanish National Research Council (CSIC) for Contract JAE-DOC 2009.

## REFERENCES

(1) Wang, Y.; Yi, J.; Xia, Y. *Adv. Energy Mater.* **2012**, *2*, 830−840.
(2) Armand, M.; Tarascon, J. M. *Nature* **2008**, *451*, 652−657.
(3) Kang, B.; Ceder, G. *Nature* **2009**, *458*, 190−193.
(4) Park, M.-H.; Kim, M. G.; Joo, J.; Kim, K.; Kim, J.; Ahn, S.; Cui, Y.; Cho, J. *Nano Lett.* **2009**, *9*, 3844−3847.
(5) Tarascon, J. M.; Delcourt, C.; Prakash, A. S.; Morcrette, M.; Hegde, M. S.; Wurm, C.; Masquelier, C. *Dalton Trans.* **2004**, *19*, 2988−2994.
(6) Huang, H.; Faulkner, T.; Barker, J.; Saïdi, M. Y. *J. Power Sources* **2009**, *189*, 748−751.
(7) Barré, M.; Crosnier-Lopez, M. P.; Le Berre, F.; Bohnké, O.; Suard, E.; Fourquet, J. L. *Dalton Trans.* **2008**, *23*, 3061−3069.
(8) Hong, H. Y. P. *Mater. Res. Bull.* **1976**, *11*, 173−182.
(9) Goodenough, J. B.; Hong, H. Y. P.; Kafalas, J. A. *Mater. Res. Bull.* **1976**, *11*, 203−220.
(10) Alami, M.; Brochu, R.; Soubeyroux, J. L.; Graverau, P.; le Flem, G.; Hagenmuller, P. *J. Solid State Chem.* **1991**, *90*, 185−193.
(11) Tran Qui, D.; Hamdoune, S.; Soubeyroux, J. L.; Prince, E. *J. Solid State Chem.* **1988**, *72*, 309−315.
(12) Morin, E.; Angenault, J.; Couturier, J. C.; Quarton, M.; He, H.; Klinowski, J. *Eur. J. Solid State Inorg. Chem.* **1997**, *34*, 947−958.
(13) Losilla, E. R.; Aranda, M. A. G.; Martinez-Lara, M.; Bruque, S. *Chem. Mater.* **1997**, *9*, 1678−1685.
(14) Catti, M.; Stramare, S.; Ibberson, R. *Solid State Ionics* **1999**, *123*, 173−180.
(15) Aono, H.; Sugimoto, E.; Sadaoka, Y.; Imanaka, N.; Adachi, G.-Y. *J. Electrochem. Soc.* **1990**, *137*, 1023−1027.
(16) Kosova, N. V.; Devyatkina, E. T.; Stepanov, A. P.; Buzlukov, A. L. *Ionics* **2008**, *14* (4), 303−311.

(17) Orliukas, A. F.; Šalkus, T.; Kežionis, A.; Dindune, A.; Kanepe, Z.; Ronis, J.; Venckute, V.; Kazlauskiene, V.; Miškinis, J.; Lukauskas, A. *Solid State Ionics* **2012**, *225*, 620−625.
(18) Vidal-Abarca, C.; Lavela, P.; Aragón, M. J.; Plylahan, N.; Tirado, J. L. *J. Mater. Chem.* **2012**, *22*, 21602−21607.
(19) Hamdoune, S.; Tran Qui, D.; Schouler, E. J. L. *Solid State Ionics* **1986**, *18−19*, 587−591.
(20) Delmas, C.; Nadiri, A.; Soubeyroux, J. L. *Solid State Ionics* **1988**, *28−30*, 419−423.
(21) Aatiq, A.; Ménétrier, M.; Croguenne, L.; Suard, E.; Delmas, C. *J. Mater. Chem.* **2002**, *12*, 2971−2978.
(22) Patoux, S.; Masquelier, C. *Chem. Mater.* **2002**, *14*, 5057−5068.
(23) Arbi, K.; Tabellout, M.; Lazarraga, M. G.; Rojo, J. M.; Sanz, J. *Phys. Rev. B* **2005**, *72*, 094302.
(24) Arbi, K.; Mandal, S.; Rojo, J. M.; Sanz, J. *Chem. Mater.* **2002**, *14*, 1091−1097.
(25) Arbi, K.; Lazarraga, M. G.; Chehimi, D. B.; Ayadi-Trabelsi, M.; Rojo, J. M.; Sanz, J. *Chem. Mater.* **2004**, *16*, 255−262.
(26) Rodríguez-Carvajal, J. *Phys. B* **1992**, *192*, 55−69.
(27) Rietveld, H. M. *J. Appl. Crystallogr.* **1969**, *2*, 65−71.
(28) Sears, V. F. *Neutron News* **1992**, *3*, 26−37.
(29) Thompson, P.; Cox, D. E.; Hasting, J. B. *J. Appl. Crystallogr.* **1987**, *20*, 79−83.
(30) Finger, L. W.; Cox, D. E.; Jephcoat, A. P. *J. Appl. Crystallogr.* **1994**, *27*, 892−900.
(31) Catti, M.; Comotti, A.; Di Blas, S.; Ibberson, R. M. *J. Mater. Chem.* **2004**, *14*, 835−839.
(32) Stauffer, D.; Aharony, A. *Introduction to Percolation Theory*; Taylor and Francis: London, 1992.